EXPERIMENTALLY DETERMINED SOLUTE RELEASE RATES FROM VARIABLY METAMORPHOSED SHALE: IMPLICATIONS FOR WEATHERING IN THE EAST RIVER WATERSHED, CO.

by

James McGuinness

A thesis submitted to the Faculty and the Board of Trustees of the Colorado School of Mines in partial fulfillment of the requirements for the degree of Master of Science (Hydrology).

Golden, Colorado

Date _____

Signed: _____

James McGuinness

Signed: _____

Dr. Alexis Navarre-Sitchler
Thesis Advisor

Golden, Colorado

Date _____

Signed: _____

Dr. Josh Sharp
Professor and Director
Hydrological Science & Engineering Program

ABSTRACT

This study investigates the variability in solute release rates from samples of shale and slate with variable lithology resulting from contact metamorphism. Mineral dissolution column experiments are used to test the hypothesis that solute release rates will vary with metamorphic grade of Mancos Shale samples collected from the East River watershed in southcentral Colorado.

To test if there is variation in solute release rates correlating to metamorphic grade in the East River watershed; flow through column experiments were performed at ambient temperatures (~ 25°C) in clear, acrylic columns with an internal diameter of 2.54 cm and a column length of 30.48 cm**.** The following synthetic rain water solution was mixed in 15 L batches: 4.07 mg $NaNO_3$, 3.24 mg NaCl, 0.35 mg KCl,1.65 mg $CaCl_2 * H_2O$, 2.98 mg $MgSO_4 * 7H_2O$, and 3.41 mg $(NH_4)_2SO$, per liter of deionized water. Lithium triazide at .05% by volume was added to the input solution to prevent bacterial growth (Neaman et al, 2004). The synthetic rain water solution was pumped through the columns and effluent samples were collected at approximately 24-hour intervals for 20-24.

Mancos Shale in the East River watershed has been impacted by contact metamorphism. Mineral compositions have been altered from this metamorphism. The East River Mancos Shale samples are separated into three qualitative groups the highest metamorphosed, moderately metamorphosed, and least metamorphosed. Compositional differences in the bulk mineralogy of metamorphosed samples compared to unmetamorphosed samples are linked to differences in the steady state release of solutes.

TABLE OF CONTENTS

LIST OF FIGURES

LIST OF TABLES

ACKNOWLEDGMENTS

I would like to thank my committee and advisor for their support, and my family for their constant encouragement.

CHAPTER 1

INTRODUCTION

Rock weathering controls important Earth surface processes. Over the long term, rates of weathering and erosion combine to control soil chemistry and evolution of landscapes (White et al., 1996; Anderson et al., 2007; Brantley and White, 2009). Chemical weathering of bedrock at the Earth's surface contributes to important Critical Zone processes such as nutrient cycling, C sequestration, erosion, and sediment transport (e.g., Drever, 2004; Brantley et al., 2007). Flux of solutes derived from silicate and carbonate rock dissolution is a control on the composition of the oceans and the atmosphere through geologic time (Maher, 2011). The balance between removal of sediments by transport processes and the breakdown of rock into movable material by weathering exerts a strong control on landscape evolution. Understanding the processes that control rock weathering susceptibility is important for predicting these processes and how perturbations to the landscape and climate propagate through the weathering system.

High elevation catchments are sensitive indicators of climate change (Winnick et al.,2017). Freshwater solute supply in mountainous is released from seasonal snow melt, making alpine catchments significant sources of water for much of the western United States (Winnick et al.,2017). As snowmelt moves through the subsurface, it accumulates solutes through chemical weathering reactions and the breakdown of organic matter (Winnick et al.,2017). The generation and export of these solutes, as well as the mixing of waters along flow paths that experience differential reaction networks and progress, exert a direct control on water quality (Todd et al., 2012). Solutes released through weathering ultimately end up in the ocean and variations in weathering through geologic time lead to variations in solute flux. Thus, improving our

understanding of water-rock interactions, weathering processes, and weathering susceptibility of these catchments at water-shed scale is critical. The controlling factors behind rock weathering processes have been studied extensively for a number of decades (Maher, 2010). Lithology is a control on how ground water moves through the subsurface, dictating flow regimes and rate of flow through porous media within hydrologic systems. Lithologic heterogeneities further complicate our understanding of rock weathering processes.

Lithology plays an important role in determining how fast rocks weather. Different minerals dissolve at different rates, thus weathering of bulk rocks is controlled by the mineral assemblage. As different minerals dissolve, the concentrations of solutes released through rock weathering can vary with lithology. One way to isolate the effects of lithology from other key weathering controls such as climate, time of surface exposure and land use is to find gradients in lithology in the same watershed. Alteration of rocks by metamorphism directly impacts rock pore structure, changing the movement in porous media and imparting changes in the rock weathering susceptibility (Maher,2011; Li et al., 2016). Changes in fluid pathways and residence time associated with metamorphism correspond to differences in solute release rates and changing river chemistry (Li et al., 2016; Maher, 2011). The relationship between weathering of rocks and water chemistry within a catchment has been the focus of previous studies (Horton et al., 1999; Gaillardet et al.,1999). These studies have compared chemical weathering rates and dissolved solute concentrations for various rock types in terrestrial watersheds, and are complicated by regional differences in several parameters, such as hydrology, climate, and vegetation (Horton et al., 1999). The weathering rates of carbonate bearing sediments can dominate in these watersheds (Horton et al., 1999). Despite these previous efforts opportunities exist to improve the understanding of watershed scale weathering and subsequent solute release

potentials. Quantitative studies of weathering potential and solute release across a lithologic gradient in a single watershed will improve the understanding of how lithology impacts solute release potentials.

Shale weathering is important because fine-grained shale and laminated sedimentary rocks constitutes about two thirds of the sedimentary record of planet Earth and a quarter of the continental land mass (Blatt,1982; Garrels and Mackenzie,1969; Hidalgo,2001; Ilgen et al, 2017; Jin et al.,2014; Rimsdtidt, 2017; Suchet et al. 2003). While the unique and heterogeneous physical characteristics of shales have made them heavily studied (Ilgen et al., 2017), knowledge of shale heterogeneity in chemistry, mineralogy and pore structure is far from complete (Barnard et al., 2012; Chen et al., 2014).The physical and chemical properties of shale are controlled by their depositional environment, post-depositional diagenetic history (Ilgen et al, 2017). Shales are volumetrically dominant in both marine and terrigenous successions and host significant portions of the fluid rock interactions controlling fate and transport of elements in the upper crust and atmosphere (Milliken, 2004). Chemical weathering of shale has been shown to serve as a long-term global sink for carbon dioxide (CO_2) storage (Jin et al.,2014). It is also well known that the lithologic heterogeneities prevalent in shales can cause spatially variable geochemical reactive transport conditions at the watershed scale (van der Zee and van Remsdijk, 1991; Barber et al., 1992; Atchley et al., 2014), ultimately impacting the spatial distribution of solute release within a watershed. Shales in high elevation catchments can be metamorphosed further complicating the impact on spatial distributions and solute release potential within a high elevation shale hosted watershed.

To our knowledge no study has evaluated how weathering potentials vary between metamorphosed and unmetamorphosed shales. Metamorphism can change the mineralogical and physical properties of rocks; these changes should propagate into the weathering system. The bedrock underlying the East River is undifferentiated Cretaceous Mancos Shale, that has been metamorphosed to varying grades by Oligocene-aged igneous intrusions. Samples for this research project were collected from sites in the East River watershed near the Rocky Mountain Biological Laboratory (RMBL) in Gothic, CO. Investigating the effects of lithology and rock properties on solute release potentials in the same watershed is possible by assuming other parameters that control weathering such as climate, time of land surface exposure and land use are approximately the same across the portion of the watershed. This combined with the variable thermal maturity of the underlying Mancos Shale makes this watershed ideal for investigating the impact of lithology and rock properties on solute release rates and water chemistry at the watershed scale in a shale-hosted system. While the metamorphism might change the hydrologic properties of the rock and the way water moves through the watershed, we are focusing this study on the release of solutes from the rock under the same hydrologic conditions. Additional future work could experimentally change the hydrologic conditions in the columns or use numerical models to evaluate how hydrologic changes propagate to changes in rock weathering and solute release at the watershed scale, these investigations are outside the current scope of this study.

The Mancos Shale underlaying the East River watershed has been altered by contact metamorphism from Oligocene-aged igneous intrusions. The changes in rock pore structure and mineralogy from these intrusions can decrease weathering susceptibility and alter the residence times and release rates of aqueous solutes (Anovitz, 2009).

1.1 Problem Statement

Here we aim to show that metamorphism affects solute release potential by measuring solute release from samples in in a variably metamorphosed shale from a single valley in Colorado. This study investigates the effects of alterations from metamorphism and weathering processes on solute release potentials by utilizing flow through column scale experiments with samples of Mancos Shale from surface outcroppings in the East River valley. The East River catchment is a mountainous, high-elevation watershed where stream flow is dominated by snowmelt in the spring and summer months and thus broadly representative of similar catchments throughout the Rocky Mountains that supply downstream water (Markstrom et al., 2012). The catchment is dominated by the Cretaceous Mancos Shale Formation, with carbonate and pyrite contents of roughly 20% and 1%, respectively (Morrison et al., 2012), and the spatially variable presence of surficial glacial and alluvial sediments (Gaskill et al., 1967, 1991; Bryant, 1969; Mutschler, 1970). The upper tributaries of the catchment are underlain by Cretaceous Mancos Formation, which varies in composition from calcareous shale to silty sand and is in contact with outcrops of Tertiary quartz monzonite. The eastern side of the catchment is underlain by a combination of Mancos Shale, Paleozoic sedimentary rocks (Morrison, Maroon, and Gothic formations) and Tertiary granodiorite (Gaskill et al, 1967, 1991; Byrant 1969; Mutschler, 1970). The Mancos Shale in the East River catchment is ideal for testing how metamorphism affects solute release potential of shale and metamorphosed shale.

CHAPTER 2

EXPERIMENTALLY DETERMINED SOLUTE RELEASE RATES FROM VARIABLY METAMORPHOSED SHALE: IMPLICATIONS FOR WEATHERING IN THE EAST RIVER WATERSHED, CO.

2.1 Introduction

Lithology plays an important role in determining how fast rocks weather. Different minerals dissolve at different rates, thus weathering of bulk rocks is controlled by the mineral assemblage. As different minerals dissolve, the concentrations of solutes released through rock weathering can vary with lithology. One way to isolate the effects of lithology from other key weathering controls such as climate, time of surface exposure and land use is to find gradients in lithology in the same watershed. Alteration of rocks by metamorphism directly impacts rock pore structure, changing the movement in porous media and imparting changes in the rock weathering susceptibility (Maher,2011; Li et al., 2016). Changes in fluid pathways and residence time associated with metamorphism correspond to differences in solute release rates and changing river chemistry (Li et al., 2016; Maher, 2011). The relationship between weathering of rocks and water chemistry within a catchment has been the focus of previous studies (Horton et al., 1999; Gaillardet et al.,1999). These studies have compared chemical weathering rates and dissolved solute concentrations for various rock types in terrestrial watersheds, and are complicated by regional differences in several parameters, such as hydrology, climate, and vegetation (Horton et al., 1999). The weathering rates of carbonate bearing sediments can dominate in these watersheds (Horton et al., 1999). It is also well known that the lithologic heterogeneities prevalent in shales can cause spatially variable geochemical reactive transport

conditions at the watershed scale (van der Zee and van Remsdijk, 1991; Barber et al., 1992; Atchley et al., 2014), ultimately impacting the spatial distribution of solute release within a watershed. Shales in high elevation catchments can be metamorphosed further complicating the impact on spatial distributions and solute release potential within a high elevation shale hosted watershed. Despite these previous efforts opportunities exist to improve the understanding of watershed scale weathering and subsequent solute release potentials. To our knowledge no study has evaluated how weathering potentials vary between metamorphosed and unmetamorphosed shales. Metamorphism can change the mineralogical and physical properties of rocks; these changes should propagate into the weathering system. Quantitative studies of weathering potential and solute release across a lithologic gradient in a single watershed will improve the understanding of how lithology impacts solute release potentials.

This study investigates the variability in solute release rates from samples of shale and slate with variable mineralogy resulting from contact metamorphism. Mineral dissolution column experiments are used to test the hypothesis that solute release rates will vary with metamorphic grade of Mancos Shale samples collected from the East River watershed in southcentral Colorado. Mancos Shale in the East River watershed has been impacted by contact metamorphism. Mineral compositions have been altered from this metamorphism. The East River Mancos Shale samples are separated into three qualitative groups the highest metamorphosed, moderately metamorphosed, and least metamorphosed.

2.2 Study Area

The East River catchment, located within the West Elk Mountain Range in southern central Colorado, is a high-elevation watershed where stream flow is dominated by snowmelt in the spring and early summer months, similar to catchments throughout the upper Colorado River Basin. Bedrock underlying the East River is Cretaceous Mancos Shale, with varying grades of contact metamorphism due to Oligocene-aged igneous intrusions. Samples for this research project were collected from sites in the East River watershed (Figure 2.1). The variable metamorphism of the Mancos Shale and lithologic gradient present in the watershed make it ideal for investigating the impact of varying degrees of metamorphism and associated lithologic and rock property changes on solute release rates and water chemistry in a watershed.

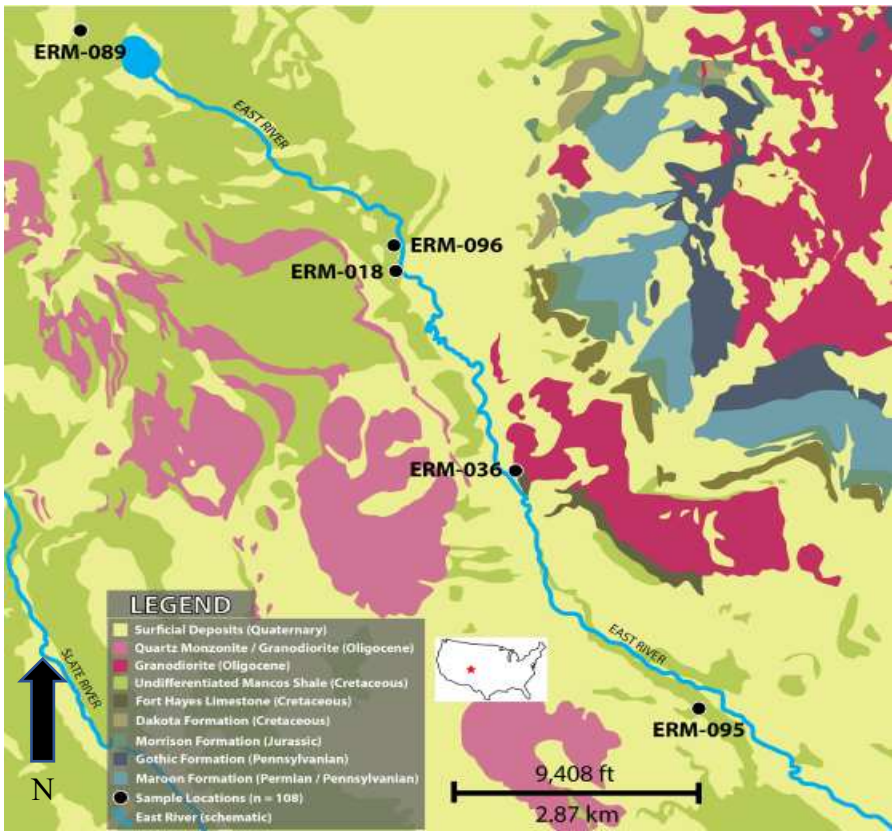

Figure 2.1 Geologic map of the East River watershed with sampling locations.

2.3 Methods

Methods are presented in the following section for sample collection and laboratory analysis for 6 column experiments. The 6 column experiments included 5 different Mancos shale samples from the East River and a control column. Columns were not performed in duplicate due the time intensive work for each column trial. Columns ran 20 to 24 days with sampling at approximately ~24-hour intervals. With the addition of the Lithium triazide at 0.05% by volume the column effluent was managed as a waste stream. Previous work demonstrated that similar columns with similar material produce data that are statistically similar and are representative of the same sample population with nonparametric Kruskal-Wallis test and Freidman tests. (Sams, 2017).

2.3.1 Sample Collection and Preparation

Samples of Mancos Shale were collected from surface outcroppings in the East River valley (Figure 2.1 p.8). After collection, all samples were crushed to a nominal size approximately 1cm x 1cm for column packing. Crushing the samples ensured fresh surface areas were exposed and that there was a uniform material size for packing. Crushed samples were dry sieved and wet sieved in deionized water with a number 10 sieve (2mm). The sieved samples were placed in 1-liter Nalgene bottles in deionized water and placed in an ultrasonicator for five minutes; the samples were then decanted through a number 10 sieve to remove excess fine material. Five-minute intervals of ultrasonication and decantation were repeated until the decanted water sieved clear. Once fine materials had been removed the samples were oven dried at 50° C for 48 hours. This sample preparation was necessary to ensure that all fine materials had been removed to prevent issues with column performance due to fine materials filling fritted

discs. The removal of fine materials also ensured that measured release concentrations were from packed shale rock and not impacted by fine materials in the columns.

2.3.2 Column Construction

Flow through column experiments were performed at ambient temperatures ~ 25°C in clear acrylic columns with an internal diameter of 2.54 cm and a column length of 30.48 cm**.** Synthetic rainwater solution was pumped through the column (4.07 mg $NaNO_3$, 3.24 mg NaCl, 0.35 mg KCl , 1.65mg $CaCl_2 * H_2O$, 2.98 mg $MgSO_4 * 7H_2O$, and 3.41 mg $(NH_4)_2SO_4$ per liter of deionized water): Lithium triazide at 0.05% by volume was added to the input solution to prevent bacterial growth. Samples were collected at approximately 24-hour intervals for all column trials run 20-24 days.

Fisher Scientific ™ FH100 and GP1000 peristaltic pumps were used to pump the synthetic rainwater into the bottom of the column at fixed flow rates of 7 mL $min^{-}1$. Samples of effluent were collected from the tubes at the top of the columns. Influent and effluent tubing was Thermo Scientific ™ All-Purpose tubing size 14. Quartz frits from Technical Glass Products qpd-25-1 were placed in the bottom and top sections between the caps and the sample to disperse flow into the column and filter any remaining fine materials. Columns were mounted vertically on ring stands and the entire system was set up away from sources of incoming light to minimize temperature fluctuations.

Columns were constructed by attaching PVC reducers to threaded brass pipes and hose barbs to the clear acrylic column. After the bottom section and fritted disc were assembled and attached to the acrylic column, shale samples were wet packed into the column.

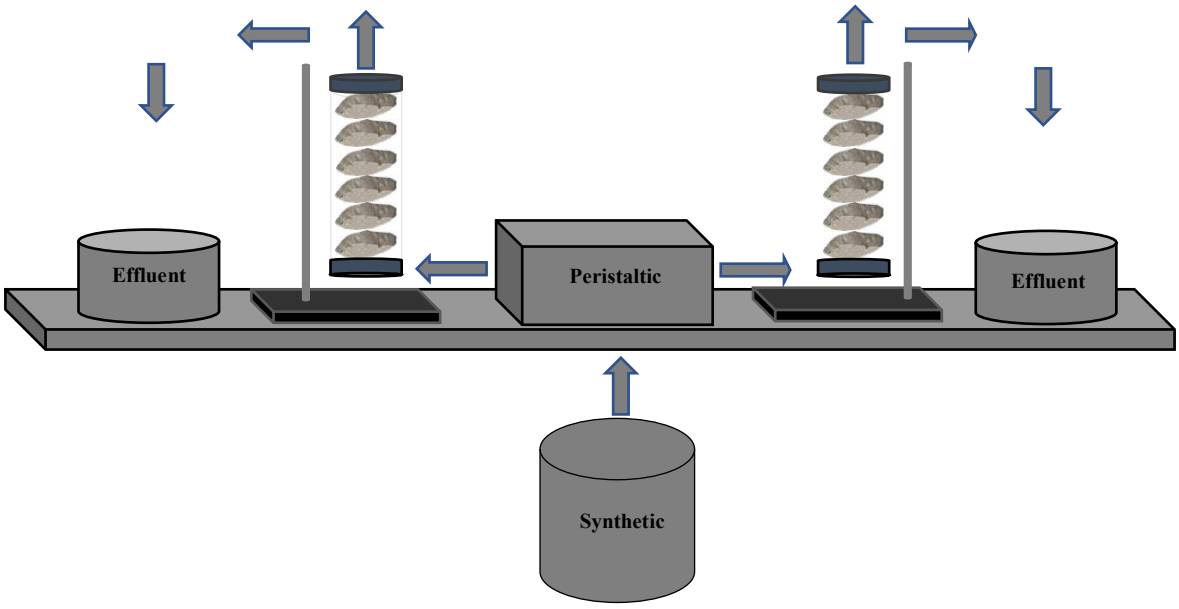

Figure 2.2 Conceptual Sketch of the flow through column experimental design.

2.3.3 Porosity and Pore Volume Calculations

The porosity (η) of each column was calculated using equation 1 where M_w (g) was the mass of water in the column determined by the difference in mass of water between saturated and dry column. V_T (cm^3) is the total volume of the column (calculated as $\pi r^2 h$ with r= 1.27 cm and h= 30.48 cm and ρ_w is the density of water (1 g cm^{-3}). The mass of water contained in the bottom section of the column was subtracted from the saturated column mass. Only accounting for the mass of water in the column section packed with shale, ensured an accurate column porosity calculation.

$$\eta = \frac{M_w}{V_T \rho_w} \tag{2.1}$$

The number of pore volumes that flowed through the column at a given time (P_T) was calculated using equation 2.2:

$$P_T = \frac{\eta V_T \rho_W}{q} \quad (2.2)$$

where T represents the time of sampling (in minutes from the start of the experiment), and q is the volumetric flow rate of water pumped in the column (mL min^{-1}). Pore volumes were calculated for comparison to similar column studies. All column experiments were run with a consistent 7 mL min^{-1} flow rate, so data were analyzed as a function of time.

The parameters for each column are show in table 2.1 (p.14) A control column with no shale was run with a 7 mL min^{-1} flow rate to measure solute concentrations of the influent solution and evaluate any release of solutes from the column materials themselves. Average influent concentrations measured from the control column were subtracted from effluent concentrations of sample packed columns. The average influent concentrations are shown in table 2.2 (p.14).

2.3.4 Sample Analysis

data from rock analysis performed on the East River Mancos Shale samples is presented in this section is. X-ray diffraction data and Cation exchange capacity was utilized along with effluent water chemistry in interpretations of results of this study. Specific surface area was utilized in BET surface area normalization of release rates.

To analyze for specific surface area, whole rock samples were hand-ground to <40 mesh (355 μm) powder (Kuila and Prasad, 2013). These powders were then analyzed using the Brunauer-Emmett-Teller (BET) nitrogen gas-adsorption method on two different Micromeritics instruments: an ASAP 2020 and a Gemini VII 2390; data were modeled with the JBH method

programmed in the Micromeritics software to calculate specific surface area (Brunauer et al., 1938).

X-ray diffraction data were collected using standard procedures for whole rock samples (Brindley and Brown, 1980; Moore and Reynolds, 1989). Samples were crushed to <0.2 mm grain size and random powder mounts were analyzed from 4° to 65° 2θ at a continuous scan rate of 2.00°/minute. MDI Jade software was used to interpret semi-quantitative mineralogy using diffractogram fitting algorithms at all sample depths.

Cation exchange capacity (CEC) was determined through a selective extractive method. Aliquots of each sample were crushed to <0.2 mm grain size utilizing an agate ball mill. A $BaCl_2$ extraction of the powdered samples was performed to account for the exchangeable fraction of metals in the weathering system (Hendershot and Duquette, 1986; Li et al., 1995; Tessier et al., 1979). These solutions were analyzed for major cation concentrations on an Inductively Coupled Plasma – Atomic Emission Spectrometer (ICP-AES). From this extraction, cation exchange capacity was calculated to compare samples across the field area.

2.3.5 Water Chemistry

Column effluent samples were collected at approximately 24-hour intervals for 20-24 days and influent concentrations were averaged from a control column trial. All samples were filtered at time of collection with a 0.45 μm nylon filter. 1% HNO_3 was used to acidify samples for cation analysis using ICP-AES analysis and Ion Chromatography with a Dionex ICS-1100.

Table 2.1 Column parameters presented by unique ID from most metamorphosed (top) to least metamorphosed.

Unique ID	Field Name	Flow Rate (mL min^{-1})	Porosity (η)	Residence Time (hours)	Total Rock (kg)
ERM-089	SH-04	7	0.69	3.38	0.218
ERM-036	GR-2	7	0.57	4.74	0.234
ERM-018	D4-F1	7	0.58	4.67	0.216
ERM-096	SH-11	7	0.62	3.76	0.218
ERM-095	SH-10	7	0.52	4.46	0.224

Table 2.2 Average influent concentrations.

ICP-AES	Average Influent [mg L^{-1}]
Ca^{2+}	0.28
K^{+}	0.34
Li^{+}	1.15
Mg^{2+}	0.17
Na^{+}	1.87
S^{2-}	1.00
Si^{4-}	0.00

Anion concentrations were measured in filtered unacidified samples with Ion Chromatography on a Dionex ICS-2100. Ca^{2+},Mg^{2+},Na^{+}, and SO_4^{2-} were determined utilizing Ion

Chromatography. Ca_T, Mg_T, Na_T, S_T, and Si_T were determined utilizing ICP-AES. Conductivity and pH were measured at the time of sampling in unacidified samples. Orion Conductivity and pH meter were calibrated to Thermo Scientific Orion buffer standards prior to sampling. Dissolved Oxygen was measured by colorimetric analysis in un-acidified samples at the time of sampling at approximately 48-hour intervals with CHEMets Dissolved Oxygen kit K-7512 self-filling ampoules. Data from the last 7 samples from each column were averaged to represent steady state effluent concentrations (figure 2.3 p. 20). Cation concentrations were determined by ICP-AES on these 7 samples from each column. Alkalinity titrations were performed from un-acidified samples for these 7 samples with a HACH digital titrator model 16900. A titration cartridge with sulfuric acid 0.1600 ± 0.0008N was used to perform the titrations with alkalinity reported as either mg L^{-1} HCO_3^- or CO_3^{2-}.

2.3.6 Steady State Solute Release Rate Calculations

In this study, steady state release rates were calculated from the average of the 7 steady state release concentrations from each column. Error was accounted for by taking the standard deviation of the 7 steady state values divided by the square root of the number of points averaged (Tellinguisen, 2001). This is shown using equation 2.3, where ε_x is the resulting error for a solute of interest (x), σ is the sample standard deviation and n is the total number of points averaged.

$$\varepsilon_x = \frac{\sigma}{\sqrt{n}} \tag{2.3}$$

The sample standard deviation was found using equation 2.4 where X_i is the value of each point in the data set and $\overline{X}$ is the average value for the data set.

$$\sigma = \sqrt{\frac{1}{n-1}\sum_{i=1}^{n}(X_i - \overline{X})^2} \quad (2.4)$$

2.4 Results

2.4.1 Sample Characterization

East River Mancos Shale samples (figure 2.1 p.8) are separated into three qualitative groups: the highest metamorphosed, moderately metamorphosed and least metamorphosed, interpreted from geologic maps (Gaskil 1991, Mutschler 1970). The proximity of these samples to intrusive complexes can be seen in the surficial geologic map (figure 2.1 p.8) but these intrusions continue in the subsurface and in the 3D are in close proximity to ERM-089, ERM-036 and ERM-018. ERM-089 is the highest metamorphosed samples. ERM-089 has the lowest TOC to CEC ratio and despite being mapped as surficial undifferentiated Mancos, lies on top of intrusive complexes and has properties of slate. ERM-036 and ERM-018 are moderately metamorphosed and have a higher TOC to CEC ratio than ERM-089 and have physical properties of slate. ERM-036 is located in a section of the watershed where the Copper Creek sill dives under the Mancos Shale and is in close proximity to this intrusion. ERM-018 is also in close proximity to Oligocene age intrusions. ERM-096 and ERM-095 are the least metamorphosed samples, they have the lowest TOC to CEC ratio and are the most removed from intrusive complexes. These two samples retain the properties of shales. All data are presented in the sample order from highest to lowest metamorphic grade. Sample characterization is presented in the following section from XRD, surface area and cation exchange capacity by sample. In Table 2.3, XRD bulk rock analysis results are reported for the 5 samples used in this study. The shales used in this study are comprised of silicate and carbonate minerals in varying

percentages. Quartz or calcite comprise the most abundant mineral in each sample ranging from 11.4 to 56.2 wt% and 0 to 48.5 wt% respectively. Dolomite was identified in samples ERM-096 and ERM-095 at 9.8 wt% and 12.6 wt% respectively. Clay minerals identified include kaolinite and illite. Pyrite was identified in samples ERM-096 and ERM-095 ranging from 1.2 to1.5 wt%. Pyrite was present at 0.5 to 0.6 wt% in the metamorphosed samples which are located closest to intrusive complexes. Calcite weight percentage decreases with metamorphic grade ERM-036 > ERM-018 > ERM-096 > ERM-095, while ERM-089 did not contain calcite in sufficient amount to be detectable by XRD. Dolomite was only identified in XRD data from the samples furthest from the intrusions that are likely un-metamorphosed.

Surface areas of the samples ranged from 1.99 to 13.5 m^2 g^{-1}. ERM-089, at the top of the watershed and resting on top of intrusive complexes, has the lowest surface area and also has the highest quartz percentage. Outcrops from where this sample are collected were very silicified and very competent. It is possible that Si rich fluids related to the magma system silicified these metamorphosed rocks.

2.4.2 Steady State

From a previous study with similar methods, steady state column effluent chemistry was defined as the point at which half or more of the first derivatives of concentration fall between (1 and -1 mg L^{-1}/day) (Sams 2017). The steady concentrations from Mancos shale samples in this study were determined to reach steady state before 40 pore volumes based on these criteria. Columns ERM-036, ERM-018, ERM-095 ran for 120 pore volumes with steady state samples averaged from 84-120 pore volumes. Columns ERM-089 and ERM-096 ran for 144 pore volumes with steady state samples averaged from 108-144 pore volumes. Column effluent

samples were initially tracked by anion and cation ion chromatography to track the column's progress to steady state (Figure 2.4 p.22). Based on these criteria ΔC_i of Ca_T, Mg_T, Na_T, S_T, Si_T where checked and all first derivatives (mg L^{-1}/day) fall between 1 and -1 (mg L^{-1}/day). Steady state estimations from the last

Table 2.3 Mineral weight percent from XRD bulk rock analysis. Shale samples are comprised of silicate and carbonate minerals in varying percentages. Data presented from most metamorphosed (left) to least metamorphosed.

Mineral	ERM-089	ERM-036	ERM-018	ERM-096	ERM-095
Quartz	56.2	11.4	28.1	33.4	35.8
Plagioclase	7.9	10.8	2.0	6.9	6.3
Muscovite	10.6	2.9	7.0	1.1	5.6
Biotite	0.0	0.1	0.2	0.0	0.0
Calcite	0.0	48.5	29.9	9.0	12.0
Dolomite	0.0	0.0	0.3	9.8	12.6
Orthoclase	9.5	6.5	5.3	6.1	0.0
Pyrite	0.5	0.6	0.5	1.2	1.5
Augite	0.0	1.8	0.6	4.4	2.0
Chlorite	4.0	5.6	5.9	2.0	1.3
Kaolinite	0.8	1.0	1.2	0.2	1.7
Illite	10.3	10.9	19.3	25.8	21.3

Table 2.4 Surface area and cation exchange capacity. Data presented from most metamorphosed (top) to least metamorphosed.

Sample ID	Surface Area (m^2/g)	Cation Exchange Capacity (meq/100g)
ERM-089	1.99	2.83
ERM-036	2.19	14.75
ERM-018	13.95	8.03
ERM-096	9.97	16.57
ERM-095	5.57	13.60

7 day were averaged to produce an average cation release concentration (mole L^{-1}). Three of the columns ran for a total of 20 days (ERM-036, ERM-018, ERM-095) and two ran for 24 days (ERM-089 and ERM-096). The control column ran for 20 days, and average influent concentrations were taken from control column anion and cation data. These steady state average release concentrations were then converted to a release rate in mole sec^{-1} (Figure 2.3 p.11).

2.4.3 Effluent Water Chemistry

ΔC_i and ΔC_i day $^{-1}$ for Ca^{2+} and Mg^{2+} were monitored to ensure analytes known to be released from Mancos Shales were approaching steady state. ΔC_i and ΔC_i day $^{-1}$ for solutes Ca^{2+} and Mg^{2+} where $\Delta C_i = C_{i(out)} - C_{i(in)}$. from ion chromatography data figures (2.4 p.22, and 2.5 p.23) respectively.

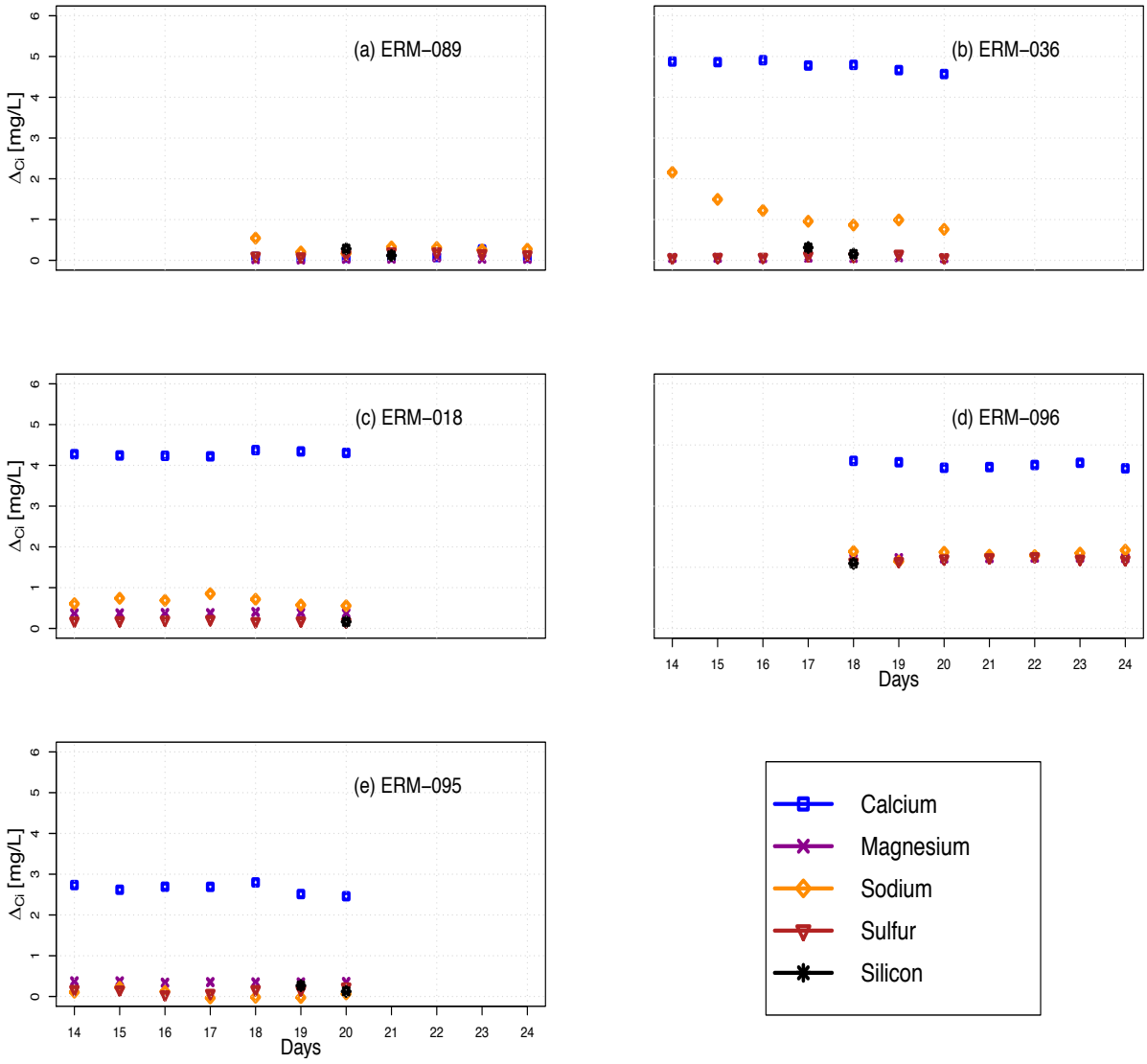

Figure 2.3 Steady state ΔC_i where $\Delta C_i = C_{i(out)} - C_{i(in)}$ i represents analytes Ca_T, MgT, Na_T, S_T, Si_T. ΔC_i used in steady state release rate calculations and normalized released rates.

Column effluents were sampled daily with pH, conductivity and concentrations over time to observe the column's progress towards steady state. pH for all columns except ERM-089 range ≈8-10 with early increases and then relatively stable pH values (figure 2.6 p.23). ERM-089 pH ranges ≈6-7(figure 2.6 p.23). Alkalinity titrations were performed for the last 7 samples of each column when the system was determined to reach steady state. Alkalinity, pH, and

concentrations from these last 7 samples were used to calculate saturation indices for calcite, dolomite, gypsum, and amorphous silica using The Geochemist Workbench™ software package and the thermo.dat database distributed with The Geochemist Workbench™ (Table 2.5 p.25).

Calcite saturation indices (SI, log Q/K_{eq}) range from -0.454 to 0.199 log Q/K , which is very close to equilibrium. Calcite SI increase with metamorphic grade for the samples with observed calcite from bulk rock analysis. For sample ERM-089 which does not contain detectable calcite, the SI is very low at -4.412 log Q/K_{eq}.

Dolomite SI range from -0.523 to 0.512 log Q/K. For sample ERM-089, which does not contain detectable dolomite the SI is very low at -7.949 log Q/K. ERM-096 and ERM-095, which do contain dolomite, have SI of -0.188 and -0.523 log Q/K and are slightly undersaturated with respect to dolomite. Samples ERM-036 and ERM-018 are moderately metamorphosed with no dolomite weight percentages observed in XRD analysis yet have dolomite SI values, of 0.202 and 0.512 log Q/K respectively. This result suggests some other source of Mg^{2+} in samples ERM-036 and ERM-018.

2.4.4 Solute Release Rates

The data from the last 7 samples from each column experimental run are representative of cation steady state release concentrations (mg L^{-1}). These steady state concentrations were converted to a concentration (mole L^{-1}) for each column (Table 2.6 p.26) Average steady state release concentrations were used in calculating an average release rate, BET normalized release rate, and mass normalized release rate.

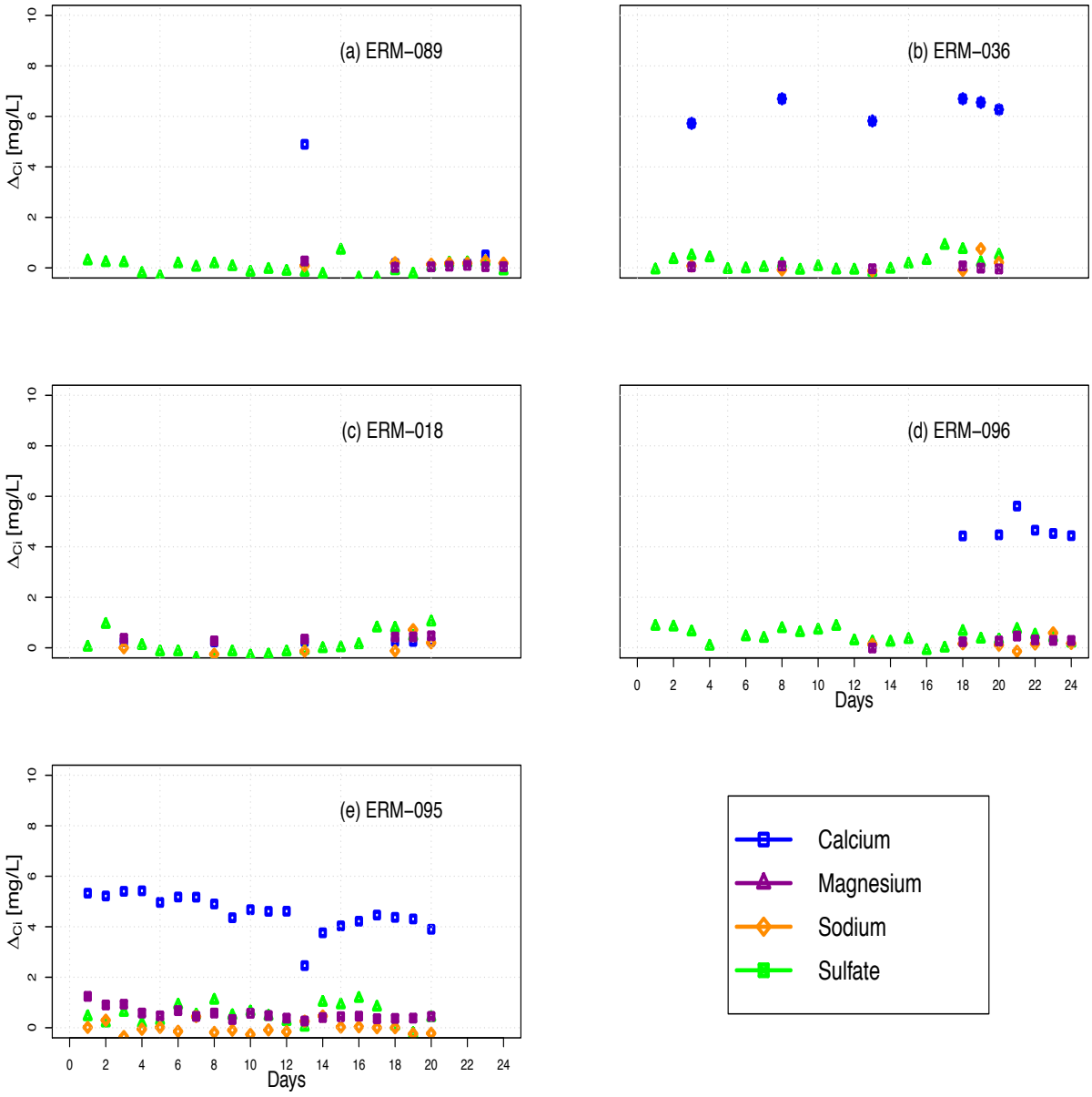

Figure 2.4 ΔC_i from IC data where $\Delta C_i = C_{i(out)} - C_{i(in)}$ i represents analytes Ca^{2+},Mg^{2+},Na^{+},SO_4^{2-}

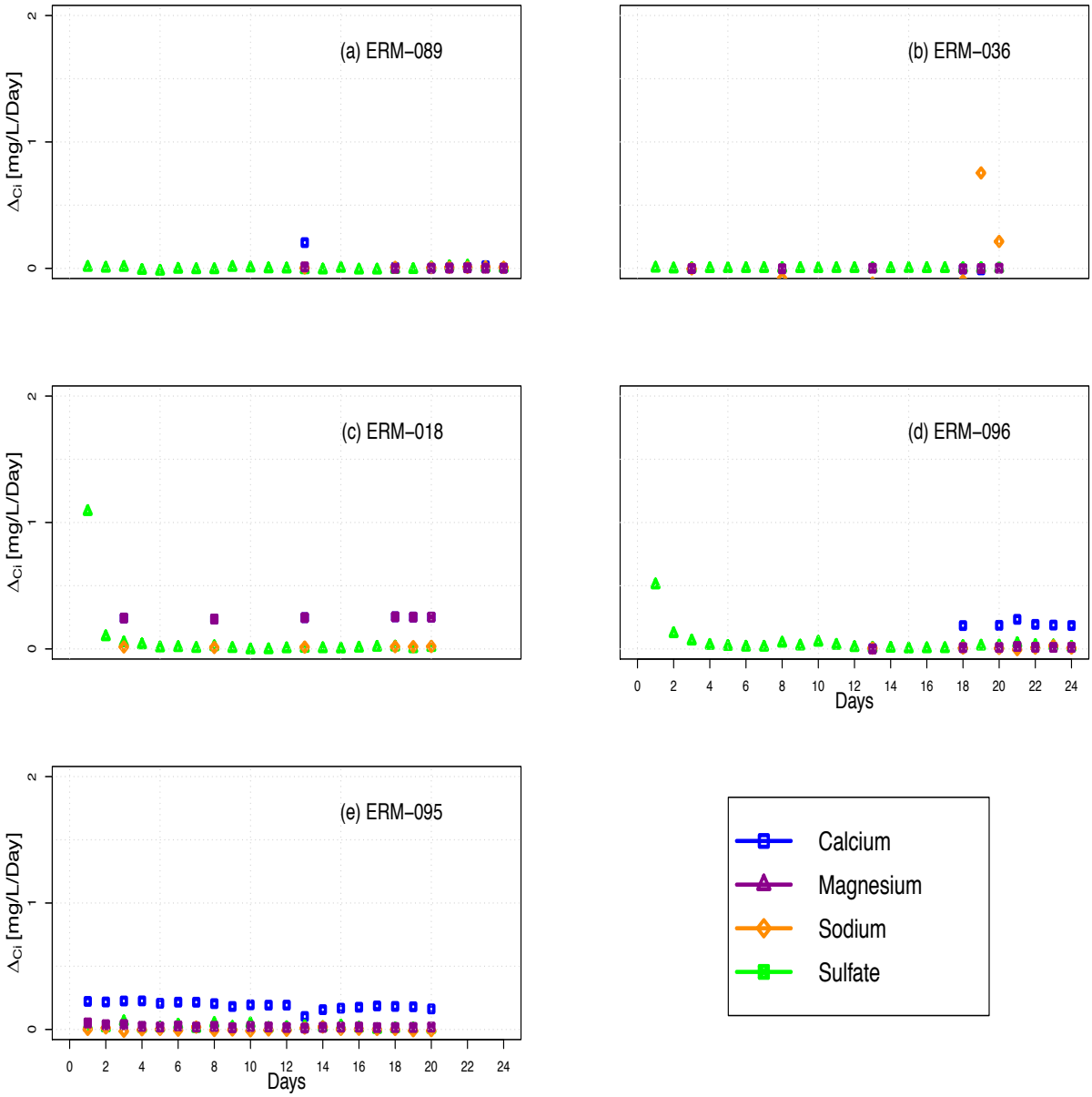

Figure 2.5 ΔC_i/day from IC data where $\Delta C_i = C_{i(out)} - C_{i(in)}$ i represents analytes Ca^{2+}, Mg^{2+} ,Na^{+} ,SO_4^{2-}.

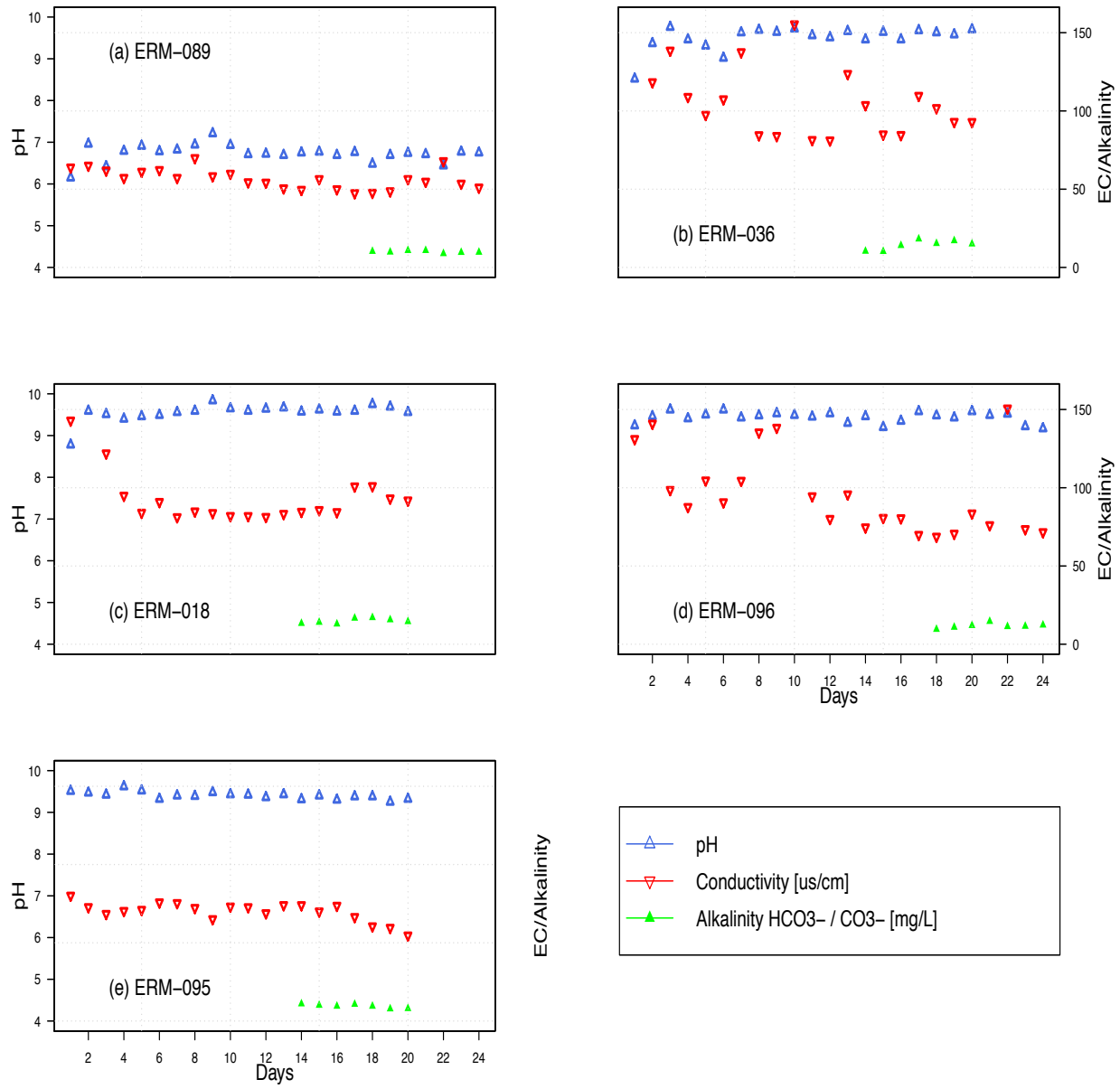

Figure 2.6 pH, conductivity and alkalinity data. Alkalinity data reported as HCO_3^- for column ERM-089 because the pH ranges ≈ 6-7, where HCO_3^- is the dominant carbonate species. Alkalinity data for all other columns reported as CO_3^{2-} because the pH ranges ≈ 8-10, where CO_3^{2-} is the dominant carbonate species.

Table 2.5 Saturation indices from Geochemist Workbench™. Data presented from most metamorphosed (top) to least metamorphosed. Averaged steady state column effluent, pH and alkalinity data were utilized with Geochemist Workbench™ software package and the thermo.dat database distributed with The Geochemist Workbench™ to calculate saturation indices..

Sample ID	Calcite (log Q/K)	Dolomite (log Q/K)	Gypsum (log Q/K)	Amorphous Silica (log Q/K)
ERM-089	-4.412	-7.949	-5.138	-2.542
ERM-036	0.199	0.202	-4.107	-3.015
ERM-018	0.148	0.512	-4.112	-2.937
ERM-096	-0.216	-0.188	-4.144	-2.884
ERM-095	-0.454	-0.523	-4.261	-2.796

2.4.5 Mass Release Rates

It is well established that not all mineral surfaces dissolve at the same rate (Lee et al., 1998; Hodson, 2006) and that potential surface area available for dissolution does not scale linearly with mass (Hodson 2006). In this study, due to discrepancies surrounding BET normalized rates (Brantley et al., 2008) and the large differences in surface area of the samples' effluent solute release rates were normalized to both mass of shale in each column and BET surface area.

Table 2.6 Average steady ΔC_i (mole L^{-1}) from the last 7 samples of each column. Data presented from most metamorphosed (top) to least metamorphosed. Average steady state ΔC_i (mole L^{-1}) used in calculating an average release rate, BET normalized release rate, and mass normalized release rate. ε represents the error for a solute of interest from equation 2.3.

	ERM-089	ERM-036	ERM-018	ERM-096	ERM-095
Ca_T	2.55×10^{-6}	1.19×10^{-4}	1.07×10^{-4}	6.60×10^{-5}	8.36×10^{-5}
K_T	2.44×10^{-5}	6.74×10^{-5}	5.41×10^{-5}	1.18×10^{-4}	4.14×10^{-6}
Mg_T	1.66×10^{-6}	2.56×10^{-6}	1.56×10^{-5}	1.24×10^{-5}	1.46×10^{-5}
Na_T	1.30×10^{-5}	5.25×10^{-5}	2.94×10^{-5}	1.86×10^{-5}	2.70×10^{-6}
S_T	4.74×10^{-6}	2.86×10^{-6}	5.87×10^{-6}	8.09×10^{-6}	4.61×10^{-6}
Si_T	7.18×10^{-6}	8.32×10^{-6}	5.78×10^{-6}	4.49×10^{-6}	6.96×10^{-6}
εCa_T	6.99×10^{-07}	2.67×10^{-06}	1.24×10^{-06}	9.12×10^{-07}	1.14×10^{-06}
εK_T	1.06×10^{-05}	6.28×10^{-05}	8.29×10^{-05}	6.70×10^{-05}	2.22×10^{-06}
εMg_T	2.70×10^{-07}	2.85×10^{-07}	4.21×10^{-07}	1.81×10^{-07}	1.91×10^{-07}
εNa_T	2.01×10^{-06}	1.33×10^{-05}	4.09×10^{-06}	1.99×10^{-06}	1.59×10^{-06}
εS_T	5.55×10^{-07}	8.95×10^{-07}	5.69×10^{-07}	7.15×10^{-07}	7.57×10^{-07}
εSi_T	6.37×10^{-07}	1.78×10^{-06}	5.37×10^{-07}	2.16×10^{-08}	5.52×10^{-07}

Bulk mass release rates R_x (mole sec^{-1}) were calculated using equation 2.3, where q is the flow rate in liters per second, $C_{in,x}$ represents the input concentration for a solute of interest x and $C_{out,x}$ represents the effluent concentration of the solute Table (2.7 p.28).

$$R_x = q[C_{out,x} - C_{in,x}] \quad (2.5)$$

Solute release rates for each Mancos Shale sample were normalized to surface areas measured with the Brunauer, Emmett, and Teller modeled N_2 gas sorption isotherms (BET). Surface area normalization is typical because weathering is proportional to the reactive surface area defined as the density of reactive sites on a silicate surface at which hydrolysis reactions occur (Brunauer et al., 1938; Brantley et al., 2005; Hodson, 2006). Steady state effluent release rates were normalized to BET surface area (mole m^{-2} sec^{-1}) using equation 2.4, where R_x is the bulk release rate from equation 3, M_R is the mass of rock in the column (kilograms) and S_{BET} is the BET surface area (m^2 g^{-1}) of a given sample (Table 8. p.28).

$$R_{BETX} = \frac{R_x}{S_{BET}} M_R \quad (2.6)$$

Steady state effluent release rates were also normalized to the total mass of Mancos Shale sample in the column (mole kg^{-1} sec^{-1}) using equation 2.5 (Table 2.9 p.29). BET normalized release rates are 4-5 orders of magnitude slower compared to mass normalized release rates. A comparison of BET and Mass normalized release rates for Ca_T and Mg_T is presented in figure 2.8.

$$R_{Mx} = \frac{R_x}{M_R} \quad (2.7)$$

Table 2.7 Average steady state bulk release rates calculated from equation 3 (mole sec^{-1}). Data presented from most metamorphosed (left) to least metamorphosed.

	ERM-089	ERM-036	ERM-018	ERM-096	ERM-095
Ca_T	2.97×10^{-10}	1.39×10^{-08}	1.25×10^{-08}	7.69×10^{-09}	9.75×10^{-09}
K_T	2.84×10^{-09}	7.86×10^{-09}	6.32×10^{-09}	1.38×10^{-08}	4.83×10^{-10}
Mg_T	1.93×10^{-10}	2.98×10^{-10}	1.82×10^{-09}	1.44×10^{-09}	1.70×10^{-09}
Na_T	1.52×10^{-09}	6.12×10^{-09}	3.43×10^{-09}	2.17×10^{-09}	3.15×10^{-10}
S_T	5.53×10^{-10}	3.34×10^{-10}	6.85×10^{-10}	9.44×10^{-10}	5.38×10^{-10}
Si_T	8.38×10^{-10}	9.70×10^{-10}	6.74×10^{-10}	5.24×10^{-10}	8.12×10^{-10}

Table 2.8 BET surface area normalized average steady state release rates (mole m^{-2} sec^{-1}). Data presented from most metamorphosed (left) to least metamorphosed.

	ERM-089	ERM-036	ERM-018	ERM-096	ERM-095
Ca_T	3.26×10^{-14}	1.49×10^{-12}	1.93×10^{-13}	3.01×10^{-13}	2.19×10^{-13}
K_T	3.11×10^{-13}	8.40×10^{-13}	9.78×10^{-14}	5.40×10^{-13}	1.08×10^{-14}
Mg_T	2.12×10^{-14}	3.19×10^{-14}	2.81×10^{-14}	5.64×10^{-14}	3.83×10^{-14}
Na_T	1.66×10^{-13}	6.54×10^{-13}	5.31×10^{-14}	8.50×10^{-14}	7.08×10^{-15}
S_T	6.06×10^{-14}	3.56×10^{-14}	1.06×10^{-14}	3.69×10^{-14}	1.21×10^{-14}
Si_T	9.18×10^{-14}	1.04×10^{-13}	1.04×10^{-14}	2.05×10^{-14}	1.83×10^{-14}

Table 2.9 Mass normalized average steady state release rates (mole kg^{-1} sec^{-1}). Data presented from most metamorphosed (left) to least metamorphosed.

	ERM-089	ERM-036	ERM-018	ERM-096	ERM-095
Ca_T	1.36×10^{-09}	5.95×10^{-08}	5.77×10^{-08}	3.53×10^{-08}	4.35×10^{-08}
K_T	1.30×10^{-08}	3.36×10^{-08}	2.92×10^{-08}	6.33×10^{-08}	2.15×10^{-09}
Mg_T	8.86×10^{-10}	1.27×10^{-09}	8.41×10^{-09}	6.61×10^{-09}	7.61×10^{-09}
N_T	6.96×10^{-09}	2.62×10^{-08}	1.59×10^{-08}	9.97×10^{-09}	1.41×10^{-09}
S_T	2.54×10^{-09}	1.43×10^{-09}	3.17×10^{-09}	4.33×10^{-09}	2.40×10^{-09}
Si_T	3.84×10^{-09}	4.15×10^{-09}	3.12×10^{-09}	2.40×10^{-09}	3.63×10^{-09}

2.5 Discussion

2.5.1 Controls on variation in mass release rates

Release of solutes and weatherability of shales has been shown to be controlled largely by mineralogy and the spatial distribution of minerals within a formation (Liermann et al.. 2011; Salehikhoo, 2013). Metamorphism and lithologic variation affect solute release potentials and rates from Mancos Shale in the East River. Shale dominated watersheds exhibit complex mineralogy and compositional variations across many scales (Jin, 2010; Liermann et al., 2011; Jin, 2014; Ma, et al., 2015; Rimstidt et al., 2017). The East River watershed has mineralogical variations due to lithology and metamorphism. The results of this study suggest that these variations affect solute release potential and rates. Alteration of rocks by metamorphism directly impacts rock pore structure, changing the movement in porous media and imparting changes in the rock weathering susceptibility (Maher, 2011; Li et al., 2016). Changes in fluid pathways and

residence time associated with metamorphism correspond to differences in solute release rates and changing river chemistry (Li et al., 2016; Maher, 2011). Contact metamorphism of the shales by granitic intrusion triggers the thermal reaction of organics, filling the macropores and microcracks of metamorphosed shales with microcrystalline quartz, ultimately decreasing the BET surface area and porosity of shales near igneous intrusions (Li et al., 2016).

Mineralogy, mineral saturation states and degree of metamorphism are controls on mass release rates in Mancos Shale. Mancos Shale samples with the highest calcite wt % and the highest Ca^{2+} SI have the fastest Ca_T mass release rates in the East River samples. ERM-089 which had no calcite present and very low SI calcite had the lowest Ca_T release rate.

Mg_T release from ERM-036 and ERM-018 is likely not related to dolomite dissolution as there was no dolomite detected in the XRD analysis. Additionally, these samples are low in Mg^{2+} in the cation exchange pool which would be another source of Mg^{2+} (Table 2.10 p.31). One potential source is Mg^{2+} contained in calcite in the metamorphosed samples. While outside the scope of this study cathodoluminescence analysis or SEM-EDS of the calcite would be able to test this hypothesis.

Moderately metamorphosed samples have the fastest release of Ca_T. Unmetamorphosed samples have the slower release rates of Ca_T compared to moderately metamorphosed samples. ERM-089 is highly metamorphosed but has not calcite present and has the slowest release of Ca_T. This study shows that when considering metamorphism and lithology in shale hosted systems, metamorphism and lithology can affect the release rate of Ca_T and Mg_T. Compositional differences in the bulk mineralogy of metamorphosed samples compared to unmetamorphosed samples are linked to differences in the steady state release of solutes figure (2.7 p.31).

Table 2.10 Mg^{2+} Cation exchange pool. Data presented from most metamorphosed (top) to least metamorphosed.

Sample ID	Mg^{2+} CEC mg/L
ERM-089	1.4
ERM-036	0.7
ERM-018	0.45
ERM-096	1.9
ERM-095	1.8

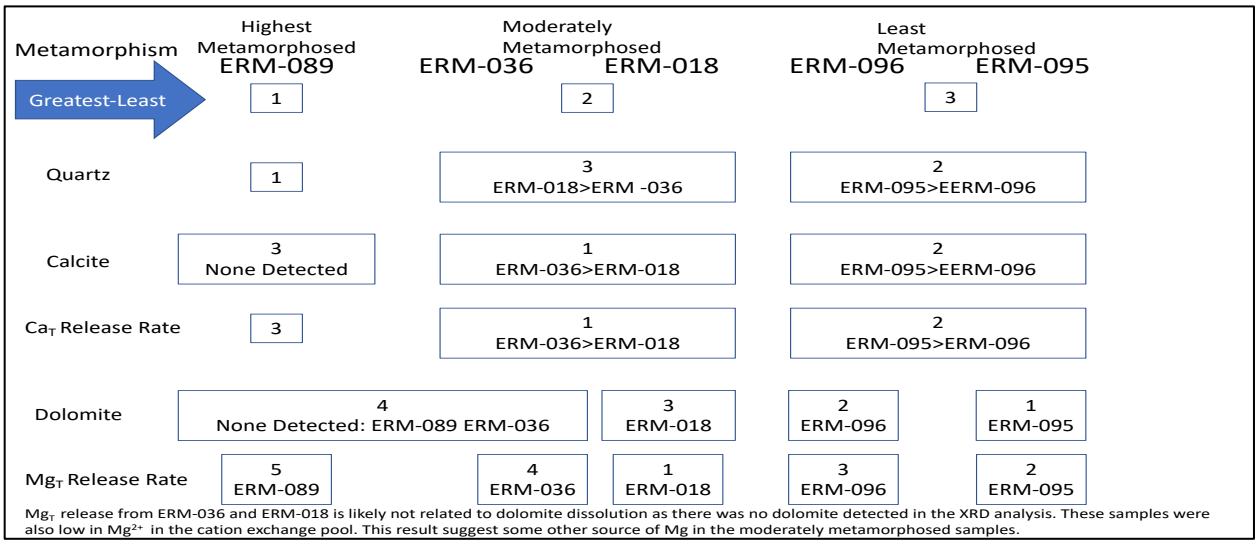

Figure 2.7 Summary of results from column experiments. Ca_T and Mg_T release rates interpreted as major release from both metamorphosed and unmetamorphosed samples. Ca_T release rate increases with metamorphic grade, however ERM-089 the most metamorphosed has no detectable calcite and thus the lowest release rate on Ca_T. Mg_T is likely not related to the dissolution of Dolomite as ERM-018 had no dolomite detected in XRD analysis and has the fastest release of Mg_T. ERM-095 and ERM-096 which had dolomite detected have the second and third fastest release respectively.

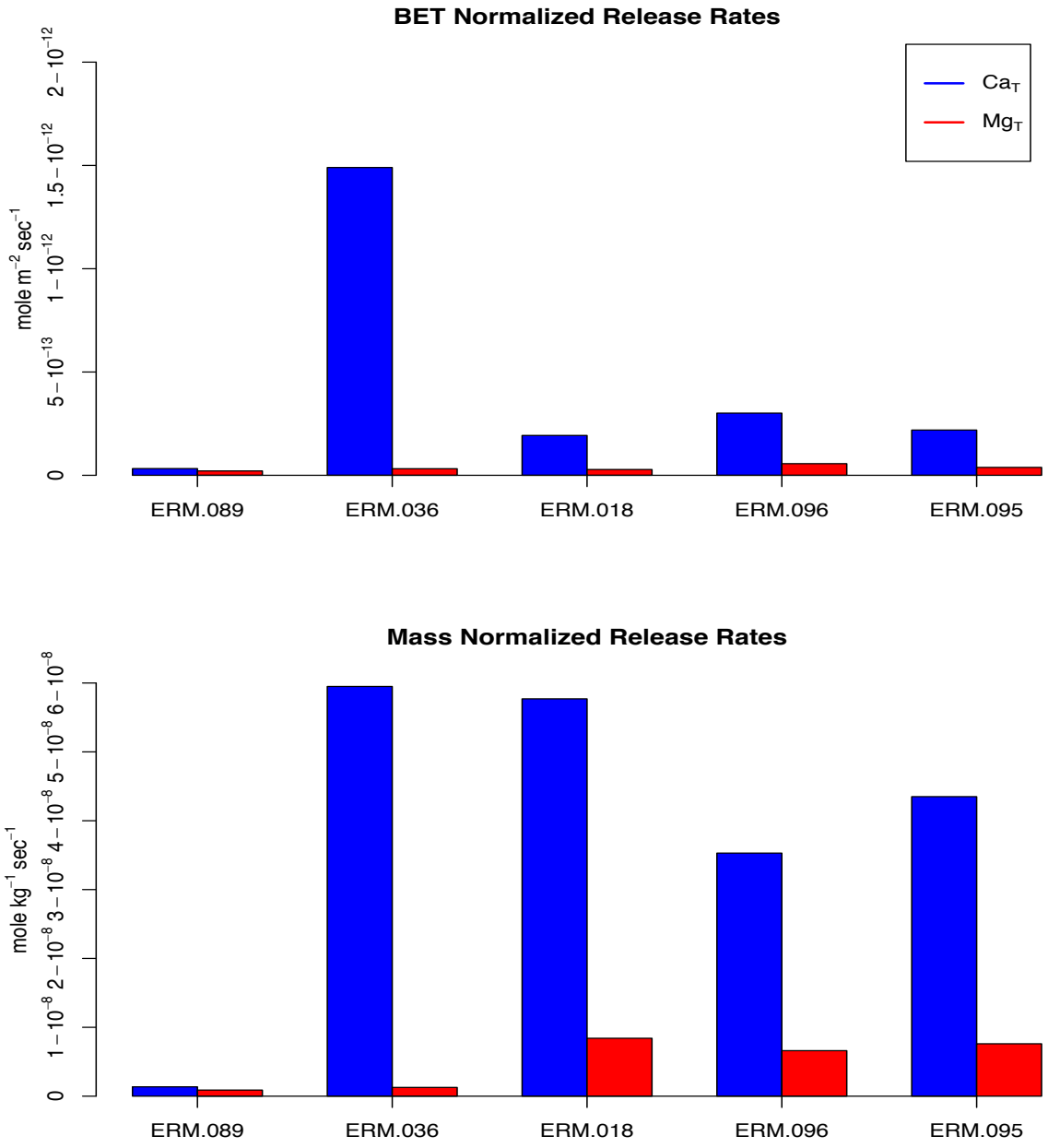

Figure 2.8 BET and Mass Normalized Rates for Ca_T and Mg_T. Data presented from most metamorphosed (left) to least metamorphosed.

2.5.2 Dissolved Oxygen

Dissolved oxygen concentrations mg L^{-1} were measured at time of sampling at approximately 48-hour intervals and this qualitative analysis of dissolved oxygen (DO) concentrations in the effluent of the columns shows some reduction in DO across the column (Figure 2.9 p.34). Samples contain both pyrite and organic carbon that could be reducing agents for oxygen along the flow path during the experiments. Redox conditions of the columns were not controlled, and influent waters were open to the atmosphere. Oxygen concentrations were measured using CHEMets self-filling ampoules to evaluate potential of pyrite and organic carbon oxidation. While some reductions in oxygen concentrations, were observed the concentrations remained at or above 3 mg L^{-1} and sulfate concentrations did not increase, thus it is inconclusive whether oxidation occurred along the flow path.

2.5.3 Comparisons to other shale studies

From a previous study with similar methods (Sams 2017) trends in solute release from both metamorphosed samples and unmetamorphosed samples showed the release rate of Ca_T to be the fastest of all solutes analyzed. This study confirms that release of Ca_T is the largest solute flux and the fastest release rate in both metamorphosed and unmetamorphosed samples with the highest releases from metamorphosed samples. Differences in the rate of release from the two unmetamorphosed samples and metamorphosed samples correlate with the mineralogical similarities between metamorphosed and unmetamorphosed sample groups. Compositional differences in the bulk mineralogy of metamorphosed samples compared to unmetamorphosed samples are likely linked to differences in the steady state release of solutes in metamorphosed samples compared to unmetamorphosed samples (Sams 2017).

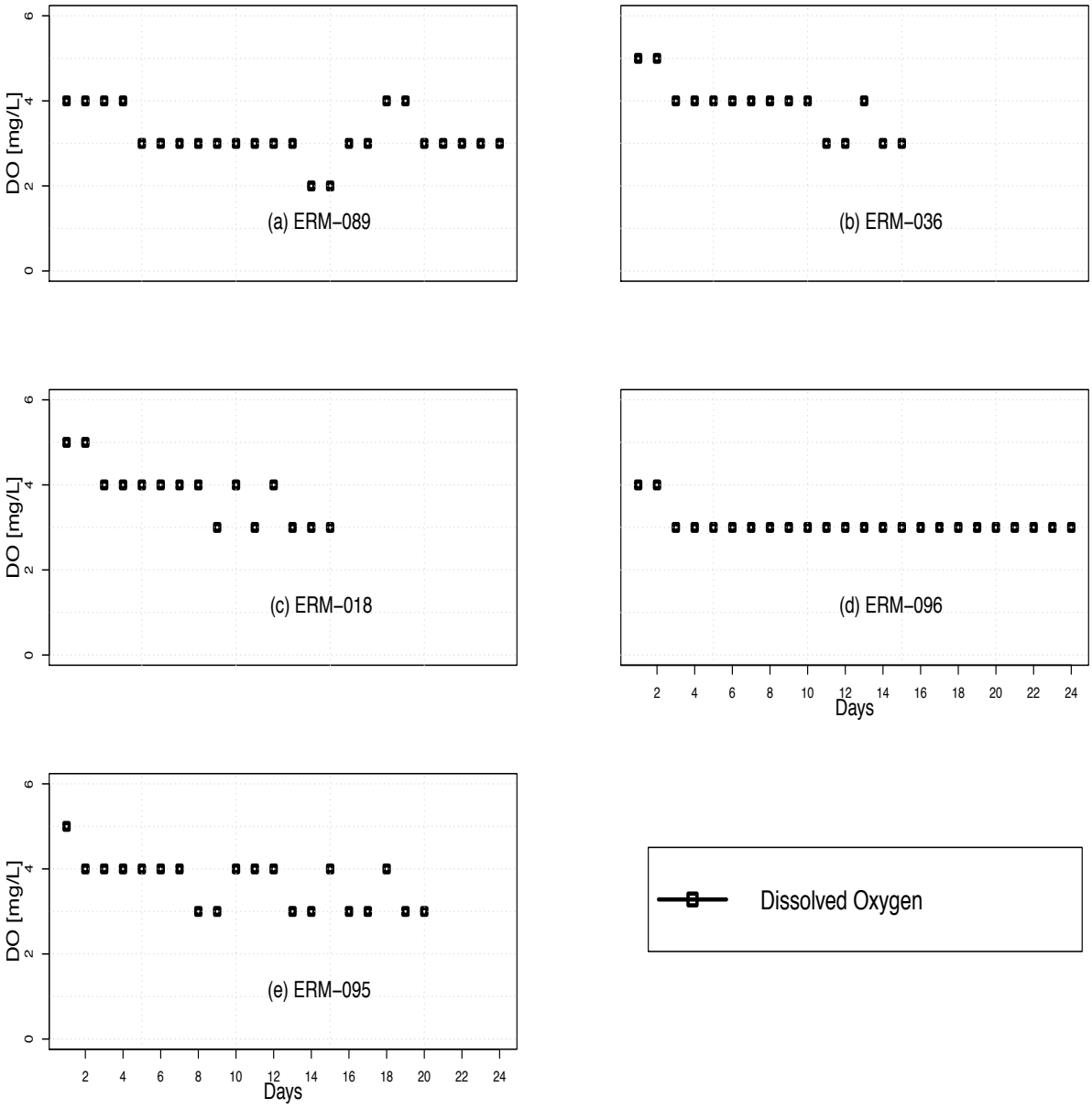

Figure 2.9 Dissolved oxygen concentrations from colorimetric analysis.

In a reactive transport model for Marcellus (black shale) to simulate shale weathering under ambient temperature and pressure conditions, constrained by soil and water chemistry data; a sensitivity analysis indicated that the most important controls on weathering include the presence of reactive gases (CO_2 and O_2), specific surface area, and flow velocity of infiltrating meteoric water (Heideri et al., 2017). The analysis emphasized the importance of specific surface area, flow velocity, and availability of CO_2 and O_2 gases in controlling regolith development.

In a study on geochemical behaviors during shale weathering, major and trace element concentrations measured in bedrock were grouped based on statistical analysis. The presence of different elemental groups was shown to be controlled by mineralogical origin, cycling processes, and geochemical properties (Ma et al., 2011). Chemical weathering reactions in this study were dominated by clay transformations specifically the weathering of illite. Shale weathering in the East River observed in this study is not dominated by clay transformations. The shale at Shale Hills Critical Zone Observatory in Penn State's Stone Valley Forest was reported 58 wt% illite. Unmetamorphosed East River samples range from 21.3 to 25.8 wt%, and metamorphosed samples range from 10.3 to 10.9 wt%. This suggests that while clay transformations play an important role in Shale Hills weathering, calcite composition across the metamorphosed Mancos Shale is dominating chemical weathering. Shale Hills elemental profiles are primarily controlled by clay dissolution despite some influence with colluvium leading to some inconsistencies in elemental compositions at depth. The various intrusive complexes in the East River valley under and in contact with the Mancos Shale make it likely that elemental concentrations and water rock interactions also vary with depth in the East River.

2.6 Conclusions

Mancos Shale in the East River watershed has been impacted by contact metamorphism. Mineral compositions have been altered from this metamorphism. Here we have shown that rocks of different metamorphic grade weather differently and release different solute concentrations at different rates. The rates of release are related to mineralogy of the samples, which appears to be related to metamorphic grade. The characteristics of mineral distribution patterns and overall mineral composition have been shown to determine the extent of water–rock interactions within a watershed (F. Salehikhoo, et al., 2015).

ERM-089 at the top of the watershed has a much larger percentage of quartz than other samples, coinciding with lowest saturation states of calcite and dolomite and the lowest release rates for Ca_T and Mg_T. Metamorphosed samples ERM-036 and ERM-018 had the highest calcite percentages and higher release rates than ERM-096 and ERM-095. XRD analysis has ultimately shown Mineralogy to be a control on Ca_T release rates and to a lesser extent Mg_T release rates. Compositional differences in the bulk mineralogy of metamorphosed samples compared to unmetamorphosed samples are linked to differences in the steady state release of solutes, specifically Ca_T in metamorphosed samples compared to unmetamorphosed samples.

CHAPTER 3

OVERALL CONCLUSIONS AND IMPLICATIONS

Solute release potential in metamorphosed Mancos Shale is related to lithologic changes associated with fluid migration through the rock during metamorphism. Where high CO_2 fluids moved through, calcite precipitated, and solute release potentials increased due to the solubility of calcite. However, in other parts of the contact aureole migrating fluids were rich in Si and rocks were silicified with little to no calcite precipitation, these rocks have low solute release potentials compared to other rocks from the contact aureole zones Mineralogy, metamorphism and weatherability are controls on solute release specifically from the dissolution of Calcite. Trends in release rates for Ca_T across metamorphosed and unmetamorphosed samples show that Ca_T release in shale hosted watersheds may be significantly higher where shale units have been altered due to metamorphism. Results of the column containing sample ERM-089 suggests that some highly metamorphosed exposed outcrops may not be actively contributing Ca_T to the watershed due to reactions that have filled the macropores and microcracks of metamorphosed shales with microcrystalline quartz, ultimately decreasing the BET surface area. ERM-089 is evidence that the changes in rock pore structure and mineralogy from these intrusions can decrease weathering susceptibility and alter the residence times and release rates of aqueous solutes. ERM-036 and ERM-018 are evidence that degrees of metamorphism and variations in lithology can increase release rates of Ca_T compared with less metamorphosed samples in a shale hosted watershed.

Although outside the scope of this study water compositions in the watershed could be compared to observed solute release and rates from column studies to show quantitatively that

weathering susceptibility in the East River is a function of metamorphism and mineral compositions of the Mancos Shale. The hypothesis that calcite in metamorphosed samples of Mancos shale is a Mg rich calcite could be investigated with cathodoluminescence analysis and SEM-EDS.

REFERENCES CITED

Aarnes I, Svensen H, Connolly JAD, Podladchikov YY (2010) How contact metamorphism can trigger global climate changes: Modeling gas generation around igneous sills in sedimentary basins. Geochimica et Cosmochimica Acta 74:7179–7195. doi: 10.1016/j.gca.2010.09.011

Anbeek C. (1992) Surface roughness of minerals and implications fordissolution studies. Geochim. Cosmochim. Acta 56, 1461–1469.

Anderson, S.P., von Blanckenburg, F., White, A.F., 2007. Physical and chemical controls on the Critical Zone. Elements 3, 315–319.

Anovitz, Lawrence M., et al. "A new approach to quantification of metamorphism using ultra-small and small angle neutron scattering." *Geochimica et Cosmochimica Acta* 73.24 (2009): 7303-7324

Atchley AL, Navarre-Sitchler AK, Maxwell RM (2014a) The effects of physical and geochemical heterogeneities on hydro-geochemical transport and effective reaction rates. Journal of Contaminant Hydrology 165:53–64. doi: 10.1016/j.jconhyd.2014.07.008

Atchley AL, Navarre-Sitchler AK, Maxwell RM (2014b) The effects of physical and geochemical heterogeneities on hydro-geochemical transport and effective reaction rates. Journal of Contaminant Hydrology 165:53–64. doi: 10.1016/j.jconhyd.2014.07.008

Barber II, L.B., Thurman, E.M., Runnells, D.D., 1992. Geochemical heterogeneity and a sand and gravel aquifer: effect of sediment mineralogy and particle size on the sorption of chlorobenzenes. J. Contam. Hydrol. 9, 35–54.

Bluth GJ, Kump LR (1994) Lithologic and climatologic controls of river chemistry. Geochimica et Cosmochimica Acta 58:2341–2359.

Brantley SL, Kubicki JD, White AF (eds) (2008) Kinetics of water-rock interaction. Springer Verlag, New York

Brantley, S.L., Godhaber, M.B., Ragnarsdottir, K.V., 2007. Crossing disciplines and scales to understand the Critical Zone. Elements 3, 307–314.

Brindley, G. W., & Brown, G. (1980). Quantitative X-ray mineral analysis of clays. Crystal structures of clay minerals and their X-ray identification, 5, 411-438.

Brunauer, S., Emmett, P. H., & Teller, E. (1938). Adsorption of gases in multimolecular layers. Journal of the American chemical society, 60(2), 309-319.

Drever, J.I. (Ed.), 2004. Surface and Ground Water, Weathering, and Soils. Holland, H.D., Turekian, K.K. (Exec. Eds.), Treatise on Geochemistry, vol. 5. Elsevier.

Gaillardet, J., Dupré, B., Louvat, P., Allègre, C.J., 1999. Global silicate weathering and CO_2 consumption rates deduced from the chemistry of large rivers. Chem. Geol. 159, 3–30.

Gaskill, D. L., F. E. Mutschler, J. H. Kramer, J. A. Thomas, and S. G. Zahony (1991), Geologic map of the Gothic quadrangle, Gunnison County, Colorado, Geologic Quadrangle Map GQ-1689, U.S. Geol. Surv., Washington, D. C.

F.E Mutschler 1970, Geologic map of the Snowmass Mountain Quadrangle Piking and Gunnison Counties , Colorado, Geologic Quadrangle Map GQ-853, U.S Geol. Surv., Washington, D.C.

Heidari P, Li L, Jin L, et al (2017a) A reactive transport model for Marcellus shale weathering. Geochimica et Cosmochimica Acta 217:421–440. doi: 10.1016/j.gca.2017.08.011

Hendershot, W. H., & Duquette, M. (1986). A simple barium chloride method for determining cation exchange capacity and exchangeable cations 1. Soil Science Society of America Journal, 50(3),605-608.

H.D. Holland, K.K. Turekian (Eds.), Treatise on Geochemistry: Sediments, Diagenesis and Sedimentary rocks, 7, Elsevier, New York (2004), pp. 159-190

Horton TW, Chamberlain CP, Fantle M, Blum JD (1999) Chemical weathering and lithologic controls of water chemistry in a high-elevation river system: Clarks Fork of the Yellowstone River, Wyoming and Montana. Water Resources Research 35:1643–1655. doi: 10.1029/1998wr900103

Ilgen AG, Heath JE, Akkutlu IY, et al (2017) Shales at all scales: Exploring coupled processes in mudrocks. Earth-Science Reviews 166:132–152. doi: 10.1016/j.earscirev.2016.12.013

Jin L, Ogrinc N, Yesavage T, et al (2014) The CO 2 consumption potential during gray shale weathering: Insights from the evolution of carbon isotopes in the Susquehanna Shale Hills critical zone observatory. Geochimica et Cosmochimica Acta 142:260–280. doi: 10.1016/j.gca.2014.07.006

Jin L, Ravella R, Ketchum B, et al (2010) Mineral weathering and elemental transport during hillslope evolution at the Susquehanna/Shale Hills Critical Zone Observatory. Geochimica et Cosmochimica Acta 74:3669–3691. doi: 10.1016/j.gca.2010.03.036

Jung H, Navarre-Sitchler A (2018) Physical heterogeneity control on effective mineral dissolution rates. Geochimica et Cosmochimica Acta 227:246–263. doi: 10.1016/j.gca.2018.02.028

Kaszuba J, Yardley B, Andreani M (2013) Experimental Perspectives of Mineral Dissolution and Precipitation due to Carbon Dioxide-Water-Rock Interactions. Reviews in Mineralogy and Geochemistry 77:153–188. doi: 10.2138/rmg.2013.77.5

Liao X, Chigira M, Matsushi Y, Wu X (2014b) Investigation of water–rock interactions in Cambrian black shale via a flow-through experiment. Applied Geochemistry 51:65–78. doi: 10.1016/j.apgeochem.2014.09.012

Liermann LJ, Mathur R, Wasylenki LE, et al (2011) Extent and isotopic composition of Fe and Mo release from two Pennsylvania shales in the presence of organic ligands and bacteria. Chemical Geology 281:167–180. doi: 10.1016/j.chemgeo.2010.12.005

Li, X., Coles, B. J., Ramsey, M. H., & Thornton, I. (1995). Sequential extraction of soils for multielement analysis by ICP-AES. Chemical Geology, 124(1-2), 109-123

Li X, Wang Q, Zhang W, Yin H (2016) Contact metamorphism of shales intruded by a granite dike: Implications for shale gas preservation. International Journal of Coal Geology 159:96–106. doi: 10.1016/j.coal.2016.03.016

Kuila, U., & Prasad, M. (2013). Application of nitrogen gas-adsorption technique for characterization of pore structure of mudrocks. The Leading Edge, 32(12), 1478-1485.

Ma, L., Chabaux, F., Pelt, E., Blaes, E., Jin, L., Brantley, S., 2010. Regolith production rates calculated with uranium-series isotopes at Susquehanna/Shale Hills Critical Zone Observatory. Earth Planet. Sci. Lett. 297, 211–225.

Ma L, Teng F-Z, Jin L, et al (2015) Magnesium isotope fractionation during shale weathering in the Shale Hills Critical Zone Observatory: Accumulation of light Mg isotopes in soils by clay mineral transformation. Chemical Geology 397:37–50. doi: 10.1016/j.chemgeo.2015.01.010

Ma L, Taylor KG, Dowey PJ, et al (2017) Multi-scale 3D characterisation of porosity and organic matter in shales with variable TOC content and thermal maturity: Examples from the Lublin and Baltic Basins, Poland and Lithuania. International Journal of Coal Geology 180:100–112. doi: 10.1016/j.coal.2017.08.002

Maher, K. (2010), The dependence of chemical weathering rates on fluid residence time, Earth Planet. Sci. Lett., 294, 101–110.

Maher K (2011) The role of fluid residence time and topographic scales in determining chemical fluxes from landscapes. Earth and Planetary Science Letters 312:48–58. doi: 10.1016/j.epsl.2011.09.040

Markstrom, S. L., et al. (2012) Integrated watershed-scale response to climate change for selected basins across the United States, U.S. Geol. Surv. Sci. Invest. Rep., 2011-5077, 143 pp.

Morrison, S. J., C. S. Goodknight, A. D. Tigar, R. P. Bush, and A. Gil (2012) Naturally occurring contamination in the Mancos Shale, Environ. Sci. Technol., 46, 1379–1387.

Milliken, 2004. Late diagenesis and mass transfer in sandstone-shale sequences. F.T. Mackenzie, H.D. Holland, K.K. Turekian (Eds.), Treatise on Geochemistry: Sediments, Diagenesis and Sedimentary rocks, 7, Elsevier, New York (2004), pp. 159-190

Moore, D. M., & Reynolds, R. C. (1989). X-ray Diffraction and the Identification and Analysis of Clay Minerals (Vol. 322, p. 321). Oxford: Oxford university press.

Nadeau PH, Reynolds RC (1981) Burial and contact metamorphism in the Mancos Shale. Clays and Clay Minerals 29:249–259.

Neaman A, Chorover J, Brantley SL (2004) Effects of organic ligands on granite dissolution in batch experiments at pH 6. American Journal of Science 306:451–473.

Salehikhoo F, Li L, Brantley SL (2013) Magnesite dissolution rates at different spatial scales: The role of mineral spatial distribution and flow velocity. Geochimica et Cosmochimica Acta 108:91–106. doi: 10.1016/j.gca.2013.01.010

Sams B, (2017) Contact Metamorphism of the Mancos Shale: Impacts on Solute Release and Weatherability in the East River Valley, Gothic, CO. M.S Thesis., Colorado School of Mines

Tessier, A., Campbell, P. G., & Bisson, M. (1979). Sequential extraction procedure for the speciation of particulate trace metals. Analytical chemistry, 51(7), 844-851.

Tellinghuisen J (2001) Statistical Error Propagation. The Journal of Physical Chemistry A 105:3917–3921. doi: 10.1021/jp003484u

Todd, A. S., A. H. Manning, P. L. Verplanck, C. Crouch, D. M. McKnight, and R. Dunham (2012), Climate-change-driven deterioration of water quality in a mineralized watershed, Environ. Sci. Technol., 46, 9324–9332.

van der Zee, S.E.A.T.M., van Remsdijk, W.H., 1991. Transport of reactive solute in spatially variable soil systems. Water Resour. Res. 23 (11), 2059–2069.

White, A.F., Blum, A.E., Marjorie, S., Schulz, M.S., Bullen, T.D., Harden, J.W., Peterson, M.L., 1996. Chemical weathering rates of a soil chronosequence on granitic alluvium: I. Quantification of mineralogical and surface area changes and calculation of primary silicate reaction rates. Geochim. Cosmochim. Acta 60, 2533–2550.

White AF (2002) Determining mineral weathering rates based on solid and solute weathering gradients and velocities: application to biotite weathering in saprolites. Chemical Geology 190:69–89.

Winnick MJ, Carroll RWH, Williams KH, et al (2017) Snowmelt controls on concentration-discharge relationships and the balance of oxidative and acid-base weathering fluxes in an alpine catchment, East River, Colorado: ACID-BASE VERSUS OXIDATIVE WEATHERING FLUXES. Water Resources Research 53:2507–2523. doi: 10.1002/2016WR019724